Laminar Jet Diffusion Flames in Microgravity: A Paradigm for Soot Processes in Turbulent Flames

by

G.M. Faeth, P.B. Sunderland, Ü.Ö. Köylü

Department of Aerospace Engineering, The University of Michigan
Ann Arbor, Michigan 48109-2140, U.S.A.

and

D. L. Urban

Microgravity Sciences Section, Sverdrup Technology, Inc.
Brook park, Ohio 44142, U.S.A.

Submitted to: International Symposium on Aerospace and Fluid Sciences (ISAFS)

Date Submitted: September 1993

Address Correspondence: G.M. Faeth
218 Aerospace Engineering Bldg.
The University of Michigan
Ann Arbor, MI 48109-2140, U.S.A.
Tel: (313) 764-7202
FAX: (313) 763-5087

Laminar Jet Diffusion Flames in Microgravity: A Paradigm for Soot Processes in Turbulent Flames

G.M. Faeth, P.B. Sunderland, Ü.Ö. Köylü

Department of Aerospace Engineering, The University of Michigan
Ann Arbor, Michigan 48109-2140, U.S.A.

D. L. Urban

Microgravity Sciences Section, Sverdrup Technology, Inc.
Brook Park, Ohio 44142, U.S.A.

Summary

An investigation of the structure and laminar smoke point properties of weakly-buoyant and nonbuoyant laminar jet diffusion flames is described. A method for predicting the structure of soot-containing flames was developed, based on the conserved-scalar formalism in conjunction with the laminar-flamelet concept. The methodology was evaluated using measurements of flame shapes, and the distributions of temperatures, mixture fractions and concentrations of major gas species, finding good agreement between predictions and measurements. Nonbuoyant flames exhibited laminar smoke points just like buoyant flames but their smoke point flame lengths and residence times were shorter and longer, respectively, than buoyant flames. These differences are caused by different soot paths in the fuel-rich region, and larger soot-oxidation/soot-formation residence time ratios for nonbuoyant than buoyant flames.

1. Introduction

Soot properties within nonpremixed flames are important because they affect the performance of propulsion systems, the hazards of unwanted fires, and the pollutant emissions from combustion processes. Motivated by these observations, the present study considered soot processes within laminar jet diffusion flames, as a computationally and experimentally tractable first step toward understanding soot processes in practical turbulent flames. Attention was confined to either weakly-buoyant flames at low pressures in normal gravity (ng) or nonbuoyant flames at normal pressures in microgravity (μg). This was done in order to investigate the differences between soot properties in nonbuoyant laminar jet diffusion flames and the more widely studied buoyant laminar jet diffusion flames, and to examine the utility of these flames as model systems for soot processes in practical turbulent flames. Two aspects of soot processes in laminar jet diffusion flames were considered, as follows: (1) the development of methods for predicting the structure of soot-containing diffusion flames, using measurements within weakly-buoyant flames to evaluate predictions; and (2) the laminar smoke point properties of nonbuoyant diffusion flames, where the predictions were used to help interpret the measurements. The following discussion of the study is brief, additional details can be found elsewhere [1-3].

The potential differences between soot processes in buoyant and nonbuoyant laminar jet diffusion flames can be attributed mainly to the different hydrodynamic properties of this flows

[4]. The differences are illustrated in Fig. 1 where some features of round buoyant and nonbuoyant laminar jet diffusion flames are plotted as a function of streamwise and radial distance, z and r, normalized by the flame length and jet exit diameter, L and d. The results for the buoyant flame are based on the measurements of Santoro et al. [5-7] while the results for the nonbuoyant flame are based on predictions to be discussed later. The regions bounded by fuel-equivalence ratios, ϕ = 1 and 2, are marked on the figure because this range of conditions is associated with processes of soot nucleation and growth [8,9]. The dividing streamline, or locus of conditions where the radial velocity, v = 0, also is shown on the plots. In particular, soot particles are too large to diffuse like gas molecules so that they are convicted by gas velocities aside from minor effects of thermophoresis. Thus, soot particles tend to move in the radial direction toward the dividing streamline. Due to flow acceleration within buoyant jet diffusion flames, the dividing streamline moves toward the flame axis with increasing z and generally lies inside the soot nucleation and growth region. In contrast, due to flow deceleration in nonbuoyant flames, the dividing streamline moves away from the flame axis with increasing z and generally lies outside the soot nucleation and growth region.

The different relative positions of the dividing streamlines and the soot nucleation and growth regions are responsible for the different soot paths in buoyant and nonbuoyant laminar jet diffusion flames illustrated in Fig. 1(excluding small regions near the axis of buoyant flames and near the base of nonbuoyant flames). For buoyant flames, soot particles first nucleate near the outer boundary of the soot nucleation and growth region (ca. ϕ = 1) and then move radically inward toward cooler and less reactive conditions at larger values of ϕ for a time before reversing direction(in ϕ space) and finally crossing the flame sheet near its tip within an annular soot layer located close to the dividing streamline. In contrast, for nonbuoyant flames, soot particles first nucleate near the inner boundary of the soot nucleation and growth region (ca. ϕ = 2) and are

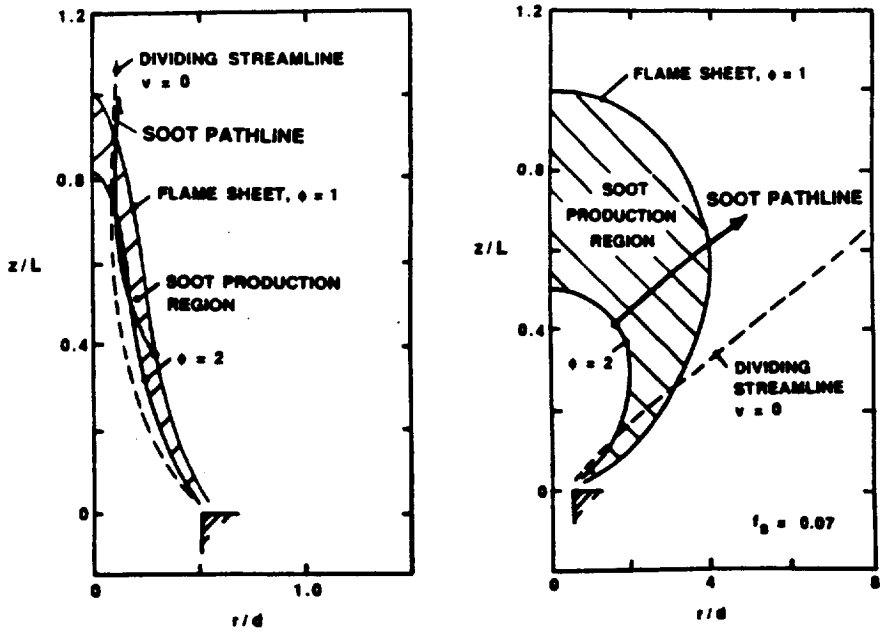

Fig. 1 Sketch of soot paths in buoyant and nonbuoyant jet diffusion flames.

drawn directly toward and through the flame sheet, experiencing a monatomic reduction of ϕ throughout their lifetime. Additionally, velocities along these two different soot paths progressively increase and decrease for buoyant and nonbuoyant flames, respectively. This implies that ratios of residence times for soot nucleation and growth to residence times for soot oxidation are generally smaller for nonbuoyant than buoyant flames. Clearly, the soot nucleation, growth and oxidation environment of buoyant and nonbuoyant laminar diffusion flames is quite different. Noting that local effects of buoyancy in turbulent flames are small, even when the flame as a whole is buoyant, this behavior suggests that nonbuoyant laminar diffusion flames provide the best paradigm for global soot processes, e.g., smoke point properties, for practical turbulent diffusion flames.

Numerous experimental studies of soot processes in buoyant laminar jet diffusion flames have been reported, see [5-9] and references cited therein. Comparable experimental information for nonbuoyant laminar jet diffusion flames is not available, however, and only can be obtained in a μg environment for flames of sufficient size to be tractable for measurements [4]. Unfortunately, complete structure measurements needed to define soot processes within diffusion flames represent a formidable task for available μg environments. Thus, reliable methods of predicting flame structure are needed, in order to supplement the limited structure measurements that can be made during typical experiments at μg [4].

Detailed numerical simulations of chemical kinetics and multicomponent transport have been successful for predicting the structure of laminar methane/air jet diffusion flames where soot concentrations are relatively low [10,11]. However, analogous methods for soot-containing flames will require significant advances in the understanding of fuel decomposition and soot chemistry. An attractive alternative involves the use of the conserved-scalar formalism, in conjunction with state relationships for scalar properties as a function of mixture fraction (called the laminar-flamelet approach), as proposed by Bilger [12]. In particular, measurements in soot-containing laminar diffusion flames show that state relationships for major gas species are relatively universal for a particular fuel burning in air [12-14], while generalized state relationships have been found for a wide variety of hydrocarbon/air flames [15]. Thus, there is potential for predicting the structure of laminar diffusion flames while avoiding the uncertainties of detailed models of the chemistry of soot-containing environments using the laminar-flamelet concept. However, effects of pressure variations on state relationships and the performance of predictions based on the laminar-flamelet approach have not been evaluated.

The laminar smoke point properties of jet diffusion flames have proven to be useful global measures of soot properties within nonpremixed flames [3,9]. Measurements of laminar smoke point flame lengths, etc., generally are based on round buoyant laminar jet diffusion flames surrounded by coflowing air, yielding results that are relatively independent of burner diameter and coflow velocities, which has helped to promote their acceptance as global measures of soot properties. Results discussed in connection with Fig. 1, however, imply that there should be fundamental differences between the laminar smoke point properties of buoyant and nonbuoyant flames which have not been explored as yet.

In view of the status of past work, the present investigation had two main objectives, as follows: (1) to complete measurements of the structure of soot-containing laminar jet diffusion flames and use the results to evaluate predictions based on the laminar-flamelet approach, and (2) to complete measurements of the laminar smoke point properties of nonbuoyant flames and to compare these results with existing measurements for buoyant flames in the literature [16-18].

2. Flame Structure

2.1 Experimental Methods. Present measurements of flame structure involved weakly-buoyant flames at ng, exploiting the fact that the effective buoyant acceleration scales as p^2g, where p is the pressure in atm and g is the normal acceleration of gravity [4]. Thus, flames at pressures on the order of 0.1 atm have effective gravitational levels of on the order of 0.01 g and are weakly-buoyant if they are not too large. Thus, present measurements involved test flames using 3 mm diameter burners that had luminous flame regions less than 50 mm long. The ambient pressure range of the tests was 0.125-0.250 atm.

The test configuration consisted of a round fuel jet injecting vertically upward, surrounded by a slow concentric flow of air. The flames burned along the axis of a vertical cylindrical enclosure having a diameter and length of 300 mm. The top and bottom of the enclosure were porous metal plates separating the enclosure from plenum chambers for air inflow and exhaust outflow which provided a uniform distribution of air over the enclosure cross section. The exit of the fuel port was 50 mm above the lower porous plate, with nearly fully-developed laminar pipe flow at the burner exit. The flames were ignited by a hot wire coil that was retracted from the burner exit once the flames were ignited and stabilized. The flames were observed using four 110 mm diameter windows located at 90° intervals around the periphery of the chamber.

Instrumentation included still photography for measurements of flame shape, thermocouples for measurements of temperature distributions in the fuel-lean portions of the flames, a radiative heat flux transducer for measurements of flame radiative heat loss fractions, gas sampling and analysis by gas chromatography to find the concentrations of major gas species and mixture fractions, laser extinction to measure distributions of soot volume fractions and laser velocimetry to measure flow velocities. Detailed descriptions and specifications of these instrument systems can be found elsewhere [1,2].

2.2 Theoretical Methods. The flame structure predictions were based on the following major assumptions: steady laminar axisymmetric flow; constant radiative heat loss fraction of the chemical energy release for all parts of the flame; the laminar flamelet approximation for all scalar properties, which requires the previous radiation approximation and implies equal binary diffusivities of all species, negligible effects of thermal diffusion and unity Lewis number; small flame stand-off distance at point of flame attachment; ambient environment has constant properties; ideal gas mixture with negligible soot volumes and a constant Prandtl/Schmidt number; and multicomponent mixing laws to find mixture viscosity. Steady laminar axisymmetric flow with constant ambient properties are conditions of the experiments while the other approximations all are aspects of the laminar-flamelet approach which is being tested [12-15].

Present measurements involved ethylene and acetylene/air flames at pressures of 0.125-0.250 atm. Thus, earlier measurements of the state relationships for these fuels burning in air atmospheric pressure [13-15] were supplemented by measurements at lower pressures during the present investigation. Typical results for acetylene/air flames are illustrated in Fig. 2 where the mole fractions, of major gas species (C_2H_2, N_2, O_2, CO_2, CO, H_20 and H_2) are plotted as a function of fuel-equivalence ratio (which is a single-valued function of the mixture fraction). The measurements extend over the pressure range 0.125-1.000 atm, drawing results at 1 atm from [14], and involve a range of burner Reynolds numbers, buoyancy conditions and positions in the flames. Predictions based on the assumption of thermodynamic equilibrium, using the Gordon

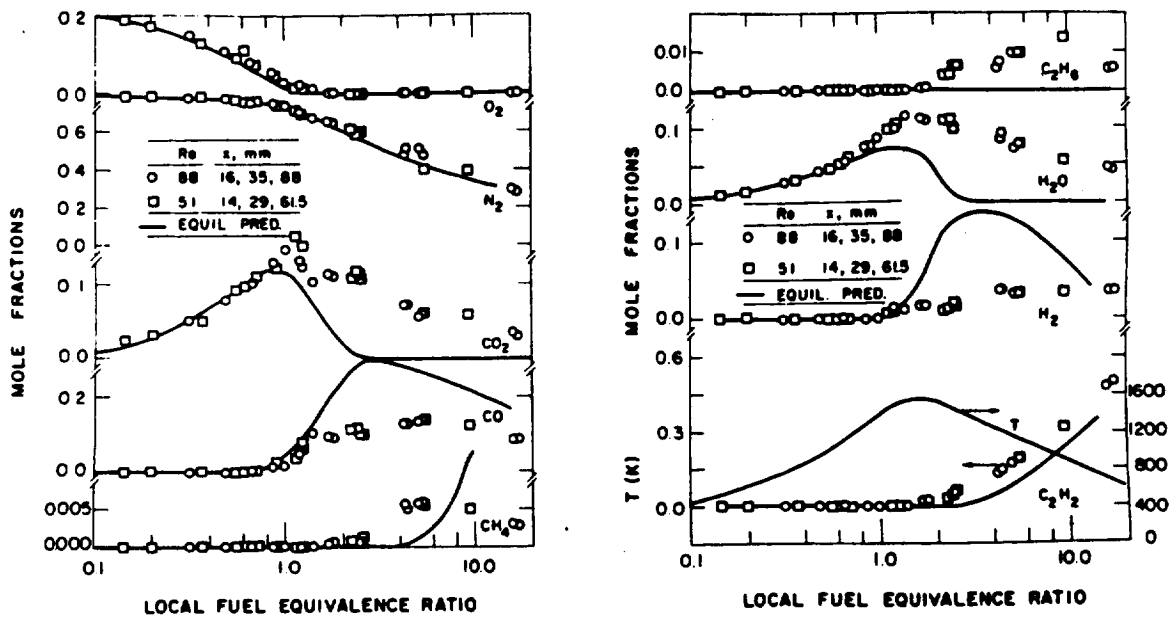

Fig. 2 State relationships for major gas species in acetylene/air diffusion flames.

and McBride [19] algorithm, also are shown on the plots. In general, the plots yield universal correlations between the concentrations of major gas species and mixture fractions, expected for the laminar flamelet concept [12-15], over the test range. The only significant exceptions are the concentrations of CO_2 and CO at fuel-rich conditions where the results of [14] are somewhat high at 1 atm for CO_2, and the present results are somewhat high for CO at 0.125 atm. On the other hand, the generalized state relationships for hydrocarbon/air flames [15] are in good agreement with the results plotted in Fig. 2, aside from the exceptions just noted. Thus, use of the same state relationships for a particular fuel/air diffusion flame appears to be acceptable over the range of pressures considered during the present investigation. Given the state relationships for major gas species, and the radiative heat loss fractions, the state relationships for temperature were computed as described in [15].

Present test conditions involved modest maximum burner exit Reynolds numbers, Re ca. 100; therefore, the full elliptic governing equations were solved rather than adopting the boundary layer approximations. Based on these assumptions the following governing equations for conservation of mass, momentum and mixture fraction must be solved:

$$\nabla \cdot (\rho \mathbf{u}) = 0 \tag{1}$$

$$\nabla \cdot (\rho \mathbf{u}\mathbf{u}) = \rho \mathbf{g} - \nabla p - \nabla \cdot (\mu \nabla \mathbf{u} + \nabla \mathbf{u}^T) \tag{2}$$

$$\nabla \cdot (\rho \mathbf{u} f) = \nabla \cdot (\mu \nabla f) / \sigma \tag{3}$$

where ρ = density, $\mathbf{u}$ = velocity vector, μ = molecular viscosity, f = mixture fraction and σ = the Prandtl/Schmidt number. The boundary conditions across the burner exit involved f = 1 by definition and fully-developed laminar pipe flow. The remaining boundary conditions allowed

for the air coflow and the chamber geometry [1,2]. The equations were solved following Patankar [20] with a variable grid spacing and a 60 (radial) × 88 (streamwise) mesh Computations for various grids indicated numerical accuracy within 1-2% [1,2].

2.3 Results and Discussion. Flame shapes were used for initial evaluation of the predictions. The predicted locations of the flames were taken to be the locus of stoichiometric conditions, $\phi = 1$; the measured flame locations were taken to be the locus of the blue-emitting flame sheet. Typical flame shape predictions and measurements for weakly-buoyant laminar jet diffusion flames are illustrated in Fig. 3. These results are for ethylene/air flames at ambient pressures of 0.125-0.250 atm and a range of burner exit Reynolds numbers. The experimental results are terminated when yellow luminosity from soot prevented observation of the blue flame boundary. Effects of buoyancy, ambient pressure and coflow are relatively weak; therefore, the main effect of reduced ambient pressures is to increase both the maximum width of the flames and the extent of the region where the blue flame sheet can be observed (the last because soot concentrations are lower at lower pressures). The comparison between predictions and measurements is good, including proper treatment of effects of Re and pressure on flame shapes, and the tendency of the flames to attach somewhat below the exit of the burner due to streamwise diffusion.

Similar plots of predicted and measured flame shapes for weakly-buoyant acetylene/air laminar jet diffusion flames at various Reynolds numbers and pressures appear in Fig. 4.

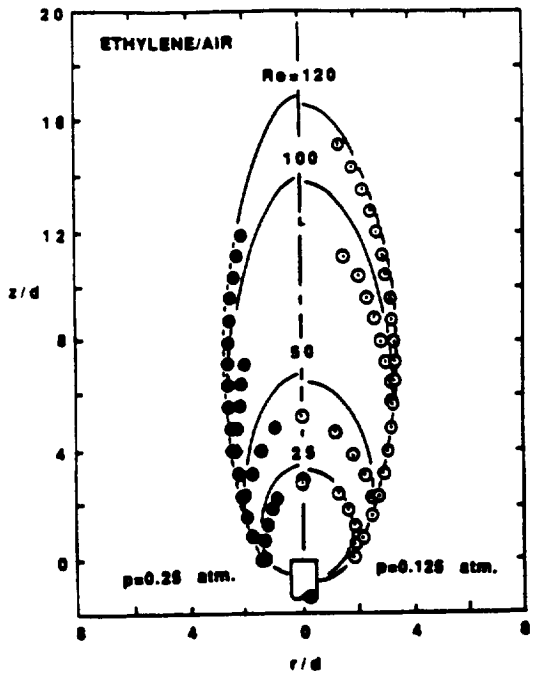

Fig. 3 Predicted and measured flame shapes of weakly-buoyant ethylene/air laminar jet diffusion flames.

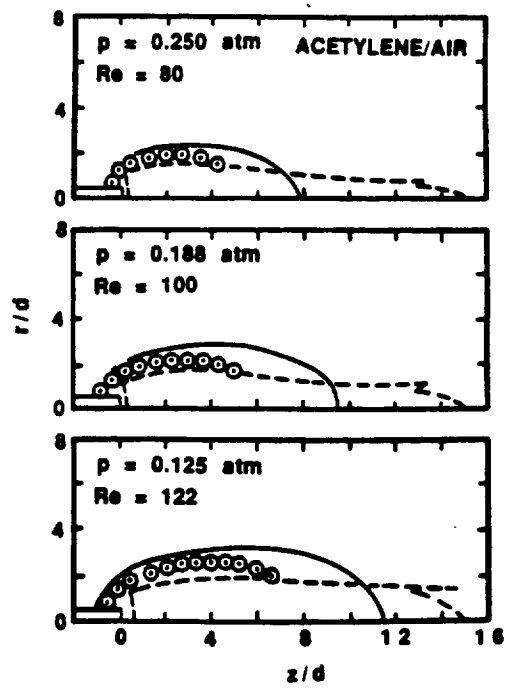

Fig. 4 Flame and luminosity boundaries for weakly-buoyant acetylene/air laminar jet diffusion flames.

Predicted flame boundaries are in fair agreement with the measurements but tend to overestimate the flame widths; this deficiency is easily removed by varying the correlation used for mixture viscosities within anticipated uncertainties for this property. Modifications of mixture viscosities in this manner have little effect on predictions of flame lengths [1,2]. The measured boundaries of the yellow soot-containing region also are illustrated in the figure. Although the visible luminosity lengths of all three flames are chosen to be similar, predicted flame lengths increase as the pressure decreases due to corresponding increases in Re. The region of soot luminosity lies inside the flame sheet near the burner exit but subsequently extends well beyond the flame tips, highlighting the extended soot oxidation region in soot-containing flames. The small "ears" near the end of the soot luminosity region also are observed in buoyant flames [16,17]; they result from the larger soot concentrations that develop in the soot layer as discussed earlier.

Predicted and measured temperature distributions in the fuel-lean region of weakly-buoyant laminar jet diffusion flames are illustrated in Fig. 5. These results correspond to the ethylene/air flames at 0.25 atm, with Re = 25, 50 and 100, illustrated in Fig. 3; however, findings at other conditions were similar. The comparison between predicted and measured temperatures is reasonably good. The main deficiencies of the predictions are slight overestimation of peak temperatures and underestimation of flow widths, which could be caused by minor disturbances of the flames due to gas motion within the enclosure.

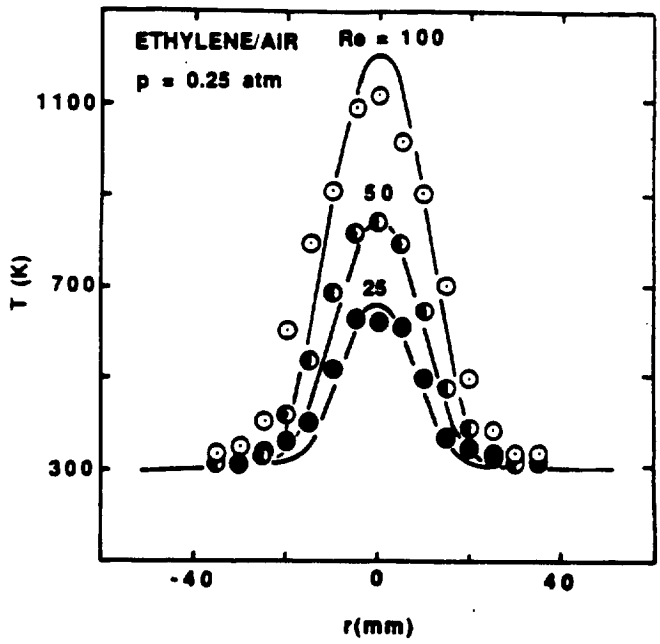

Fig. 5 Predicted and measured temperature distributions in the fuel-lean region of weakly-buoyant ethylene/air laminar jet diffusion flames.

The final evaluation of the laminar-flamelet approach involved velocity, mixture fraction and major gas species concentrations along the axis of weakly-buoyant laminar jet diffusion flames. Typical results are illustrated in Fig. 6 for an acetylene/air flame at 0.25 atm and Re = 80, which corresponds to one of the flames considered in Fig. 4. In general, the agreement between predictions and measurements is excellent, even though the region considered contains soot, cf. Fig. 4. In particular, the state relationships properly account for the low levels of oxygen observed before the fuel is completely consumed, followed by more rapid growth of oxygen concentrations beyond the flame tip. As noted in connection with Fig. 4, the location of the flame tip is predicted accurately because the predicted distribution of mixture fractions is in good agreement with the measurements. The velocity profiles highlight some of the problems of observing nearly nonbuoyant flames of reasonable size at ng. Near the jet exit, velocities decay rapidly, which is consistent with nonbuoyant laminar jet diffusion flame behavior. However, farther from the jet exit, velocities slowly begin to increase as effects of buoyancy become more significant. The predictions represent this behavior reasonably well, however, the measurements clearly are not representative of truly nonbuoyant flame behavior.

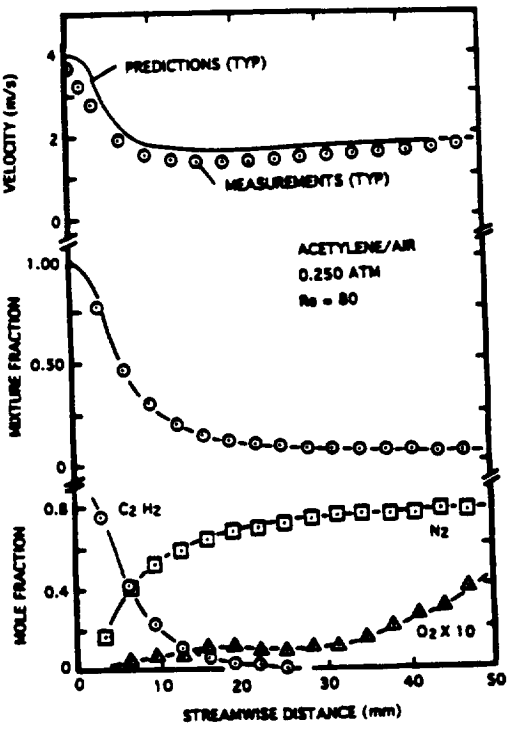

Fig. 6 Predicted and measured velocities, mixture fractions and major gas species concentrations along the axis of a weakly-buoyant acetylene/air laminar jet diffusion flame.

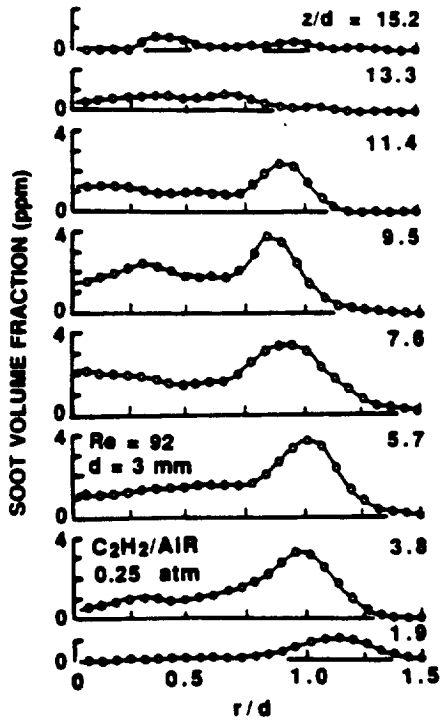

Fig. 7 Measured soot volume fraction distributions for a weakly-buoyant acetylene/air laminar jet diffusion flame at 0.25 atm.

Soot concentrations within the acetylene/air flame considered in Fig. 6 are illustrated in Fig. 7. The results involve plots of soot volume fractions as a function of radial distance at various heights above the burner exit. The annular soot layer is quite evident near the burner exit, with soot building up later near the axis as the flame tip is approached (ca. z/d = 7-9, see Figs. 4 and 6). Soot oxidation extends to the axis beyond the flame tip, with soot concentrations becoming small at all radial distances far from the burner exit in this nonsooting flame.

Taken together, results discussed in Figs. 3-7 have two main implications. First of all, the evaluation of the laminar-flamelet approach for predicting the structure of soot-containing flames appears to be promising, and offers a way of circumventing current uncertainties about fuel decomposition and soot chemistry in soot-containing flames that would be required for more detailed simulations. Secondly, the soot oxidation region of weakly-buoyant diffusion flames is quite extended, so that the end of the luminous region if almost twice as long as the flame length (based on ϕ =1 at the axis). These observations will be exploited to help interpret the laminar smoke point properties of nonbuoyant flames, to be discussed next.

3. Laminar Smoke Point Properties

3.1 Experimental Methods. The laminar smoke point properties of nonbuoyant laminar jet diffusion flames were measured using the NASA KC-135 μg facility. This aircraft flies parabolic trajectories that provide roughly 20 s at μg conditions. The experiments involved laminar ethylene and propane jet diffusion flames burning in nearly still air (10% maximum oxygen consumption by volume) within a closed windowed chamber. The chamber was cylindrical with an internal volume of 87 liters. The chamber volume can be nearly evacuated by venting overboard, due to the altitude of the aircraft, and was refilled with compressed air stored in cylinders to control levels of vitiation. The chamber was fitted with two windows and an interior light for laminar smoke point determinations. The chamber pressure was measured with an absolute pressure gage.

Three round burners (1.6, 2.7 and 5.9 mm dia.) were tested, with fully-developed laminar pipe flow at the burner exit. Fuel was delivered from storage bottles through solenoid and metering valves. The flames were ignited using retractable hot wire coils, similar to the weakly-buoyant flame tests.

The appearance of the flames was recorded by a color video camera. This allowed post-flight determination of flames disturbed by departures from the parabolic flight path so that observations at such conditions could be eliminated. The video records also were used to measure flame lengths, which were taken to be the length of the visible luminous portion of the flames. Flame lengths were found by averaging video records after fully-developed flame shapes were reached, which required roughly 2s. Sooting conditions were identified by the appearance of a dark soot streak projecting from the flame tip. The chamber pressure and the observations of soot emission from the flames were recorded orally by two observers at different view ports, using the audio channel of the video recorder.

The flame lengths measured at the onset of sooting actually were flame luminosity lengths, which is the definition used for the laminar smoke point flame lengths of buoyant laminar jet diffusion flames [3,9,16-18]. Similar to the results illustrated in Fig. 4, however, the luminosity length is longer than the conventional flame tip where ϕ =1. Fortunately, the ratios of conventional to luminous flame lengths at the laminar smoke point are similar for buoyant and nonbuoyant flames, ca. 0.6 [2,3,6,7]; therefore, the luminous flame length provides a reasonable basis to compare the sooting properties of nonbuoyant and buoyant flames.

Results for roughly ten flight parabolas were used to find laminar smoke point luminosity lengths for a given fuel, burner diameter and pressure. Based on the accuracy of the flame luminosity length determinations, potential errors due to acceleration-induced flame tilt along the camera axis and the range of conditions between nonsooting and sooting flames, the experimental uncertainties (95% confidence) of the laminar smoke point luminosity lengths are estimated to be less than 15%. The measurements were repeatable within this range.

3.2 Theoretical Methods. Laminar smoke point residence times are a useful measure of the sooting properties of a fuel. This is particularly true for nonbuoyant flames where residence times vary considerably with varying burner diameter for a given flame length, in contrast to buoyant flames where flame lengths and residence times are correlated closely and are relatively independent of the burner diameter [9,17]. Laminar smoke point residence times (defined as the time between termination of fuel flow into the base of the flame and the disappearance of all flame luminosity) have been measured directly for buoyant flames [17]. Similar results, however, were not available for the present nonbuoyant flames. Thus, the residence times for the nonbuoyant flames were found using the laminar-flamelet approach discussed earlier. For these computations, the flame residence time was defined as the time required for a fluid parcel to convect along the flame axis to the flame sheet (where $\phi = 1$).

Predictions of typical flame residence times, t_r, for nonbuoyant laminar jet diffusion flames, are illustrated in Figs. 8 and 9. These results are for ethylene/air flames at 1 atm, however, findings for propane/air flames are essentially the same. Additionally, residence times are nearly proportional to pressure for a given flame length. The results illustrated in Fig. 8 show that increasing flame lengths for a fixed burner diameter yield progressively increasing residence times. This behavior is qualitatively similar to buoyant flames, where residence times are proportional to the square root of the flame length [9,17]. However, this behavior differs from constant property estimates of flame lengths based on the boundary layer approximations, where

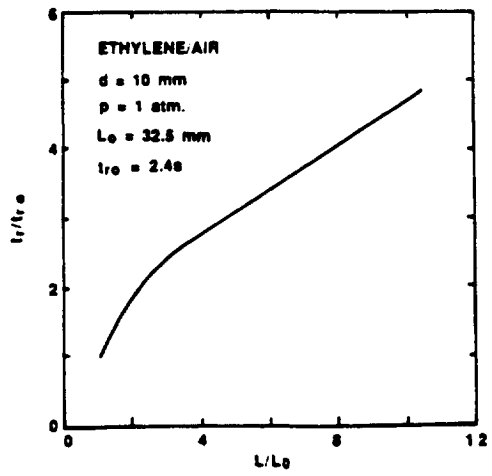

Fig. 8 Predicted flame residence times as a function of flame length for nonbuoyant ethylene/air laminar jet diffusion flames.

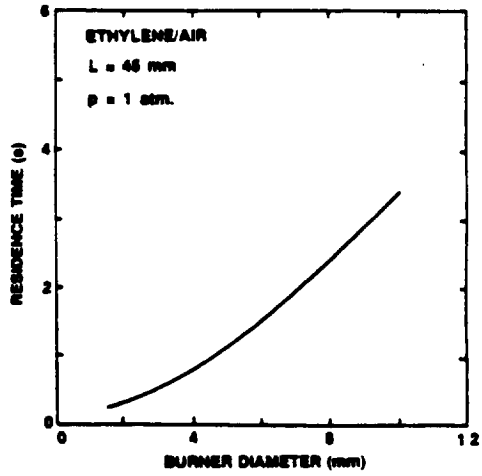

Fig. 9 Predicted flame residence times as a function of burner diameter for nonbuoyant ethylene/air laminar jet diffusion flames.

residence times are independent of flame length and only vary with burner diameter [9,21]. This difference primarily is caused by effects of diffusion in the streamwise direction at the modest values of Re associated with laminar smoke point luminosity lengths.

Results illustrated in Fig. 9 show that residence times increase with increasing burner diameter for a fixed flame length. This behavior also is observed for simplified boundary layer treatments of nonbuoyant laminar jet diffusion flames and is caused by reduced flow velocities at the burner exit as the burner diameter is increased for a fixed flame length [21]. Such behavior, however, differs from buoyant laminar jet diffusion flames where residence times largely are a function of flame length, and are relatively independent of burner diameter and exit velocity because buoyancy mainly controls velocities within these flame [9, 17,21].

3.3 Results and Discussion. Measured laminar smoke point luminosity lengths for ethylene and propylene/air diffusion flames are summarized in Table 1. Present results for nonbuoyant flames involve pressures of 0.5, 1.0 and 2.0 atm with burner diameters of 1.6, 2.7 and 5.9 mm. Results for buoyant flames are from the measurements of Refs. [16] and [17] at atmospheric pressure for a burner exit diameter of roughly 10 mm, although effects of burner diameter on the laminar smoke point properties of buoyant flames are small, as noted earlier.

There are several interesting features of the results summarized in Table 1. First, the nonbuoyant flames exhibit laminar smoke point luminosity lengths, in contrast to the conjecture that these lengths would not exist because nonbuoyant flames have residence times that are independent of flame length under the boundary layer approximations [9]. The latter behavior does not occur because streamwise diffusion causes residence times to increase as flame length increases, as discussed in connection with Fig. 8. Next, the laminar smoke point luminosity lengths of nonbuoyant flames exhibit little variation with burner diameter, similar to buoyant flames [3]. This behavior is expected for buoyant flames but not for nonbuoyant flames as discussed in connection with Fig. 9. Additionally, laminar smoke point luminosity lengths are roughly four times smaller for nonbuoyant flames than buoyant flames at otherwise comparable conditions. On the other hand, laminar smoke point residence times are much longer for

Table 1. Laminar Smoke Point Luminosity Lengths (mm)[a]

Fuel	Buoyancy	Burner Diameter (mm)	Pressure (atm)		
			0.5	1.0	2.0
Ethylene	μg	1.6	85	36	—
	μg	2.7	80	25	13
	μg	5.9	110	28	13
	ng	10.0	—	106-135	—
Propane	μg	1.6	130	42	16
	μg	2.7	140	38	18
	μg	5.9	130	42	20
	ng	10.0	—	162-169	—

[a]Found from round laminar jet diffusion flames in still air at μg, and in coflowing air from Schug et al. [16] and Sivathanu and Faeth [17] at ng.

nonbuoyant than buoyant flames, e.g., 200-1500 ms for nonbuoyant flames at atmospheric pressure, based on the predictions discussed in connection with Figs. 8 and 9, in comparison to 40-50 ms for the same fuels in buoyant flames [17].

Other properties of the laminar smoke point luminosity lengths summarized in Table 1 are qualitatively similar for nonbuoyant and buoyant flames. For example, laminar smoke point luminosity lengths are slightly longer for propane than for ethylene in both cases. Additionally, the pressure variation of laminar smoke point luminosity lengths for buoyant flames found by Flower and Bowman [18], ~ $p^{-1.3}$, agrees with trends of present measurements for nonbuoyant flames with an average error of 25%. This quantitative agreements probably is somewhat fortuitous, however, due to the different soot paths in buoyant and nonbuoyant flames discussed earlier. Nevertheless, the reduction of laminar smoke point luminosity lengths with increasing pressure is consistent with increased residence times at higher pressures for nonbuoyant flames, with effects of pressure on reaction rates being a contributing factor.

The reasons for the differences between the laminar smoke point properties of nonbuoyant and buoyant laminar jet diffusion flames are not quantitatively understood at present. However, the two general phenomena discussed earlier — different soot paths and different velocity distributions along soot paths for nonbuoyant and buoyant flames — undoubtedly play a role in this behavior. Different sites for initial soot nucleation and different conditions for subsequent soot nucleation and growth, should lead to different maximum primary soot particle sizes for nonbuoyant and buoyant flames of comparable length. The longer soot oxidation period relative to the soot nucleation and growth period for nonbuoyant flames in comparison to buoyant flames, due to different velocity distributions along soot paths, also provides a mechanism for increased residence times prior to soot emission for nonbuoyant flames. Different residence times also influence radiative heat losses and thus temperature distributions in the flames as well. Thus it is not surprising that the soot emission properties of nonbuoyant and buoyant laminar jet diffusion flames differ. It also is clear that nonbuoyant laminar jet diffusion flames provide an interesting new perspective to gain a better understanding of soot mechanisms in diffusion flame environments.

4. Conclusions

The structure and soot properties of nonbuoyant and buoyant laminar jet diffusion flames have been studied. The major conclusions of the study are as follows:

1. State relationships for major gas species concentrations within soot-containing diffusion flames of hydrocarbons and air remained relatively independent of pressure for the range 0.125-1.000 atm. This behavior simplifies application of the laminar-flamet concept for structure predictions of soot-containing laminar diffusion laminar diffusion flames.

2. The conserved-scalar formalism, in conjunction with the laminar-flamelet concept, yielded predictions of the structure of soot-containing laminar jet diffusion flames that agreed with measurements within experimental uncertainties. The approach is helpful because it circumvents current uncertainties about fuel decomposition and soot chemistry that are needed for predictions based on more detailed models treating finite-rate chemistry and multicomponent transport.

3. Nonbuoyant flames exhibit laminar smoke points, and the propensity of a fuel to soot (evidenced by variations of laminar smoke point luminosity lengths with fuel type and

pressure) is similar for nonbuoyant and buoyant flames. However, laminar smoke point luminosity lengths are much shorter, and laminar smoke point residence times are much longer, for nonbuoyant than buoyant flames.

4. Differences between the laminar smoke point properties of nonbuoyant and buoyant diffusion flames are not quantitatively understood, however, different soot paths and velocity distributions along the soot paths for nonbuoyant and buoyant flames are probably responsible for this behavior. In view of these differences, nonbuoyant laminar flames are the proper paradigm for soot processes in practical turbulent flames, which generally are not strongly affected by buoyancy.

Acknowledgments

This research was supported by the United States National Aeronautics and Space Administration (NASA) under grant no. NAG3-1245 and the Office of Naval Research under grant no. N00014-93-0321. The assistance of S. Mortezavi and C.-K. Lin of the University of Michigan with computations and instrument development is gratefully acknowledged. The authors also wish to thank J.B. Mullins, of NASA Marshall Space Flight Center, and D.J. Gotti, H.D. Ross, R.G. Sotos and D.P. Stocker, all of NASA Lewis Research Center, for assistance in carrying out the KC-135 μg tests.

References

[1] S. Mortezavi, P.B. Sunderland, J. Jurng, Ü.Ö. Köylü and G. M. Faeth: Structure of Soot-Containing Laminar Jet Diffusion Flames, AIAA Paper No. 93-0708, 1993.

[2] Ü.Ö. Köylü, P.B. Sunderland S. Mortezavi and G.M. Faeth: Soot Nucleation and Growth in Weakly-Buoyant Laminar Jet Diffusion Flames, AIAA Paper No. 94-0428, 1994.

[3] P.B. Sunderland, S. Mortezavi, G.M. Faeth and D.L. Urban: Laminar Smoke Points in Nonbuoyant Jet Diffusion Flames, Combust. Flame, in press.

[4] C.K. Law and G.M. Faeth: Opportunities and Challenges of Combustion in Microgravity, Prog. Energy Combust. Sci, submitted.

[5] R.J. Santoro, H.B. Semerjian and R.A. Dobbins: Soot Particle Measurements in Diffusion Flames, Combust. Flame Vol. 51 (1983), pp. 203-218.

[6] R.J. Santoro and H.G. Semerjian: Soot Formation in Diffusion Flames: Flow Rate, Fuel Species and Temperature Effects, Twentieth Symposium (International) on Combustion, The Combustion Institute, Pittsburgh, 1984, pp. 997-1006.

[7] R.J. Santoro, T.T. Yeh, J.J. Horvath and H.G. Semerjian: The Transport and Growth of Soot Particles in Laminar Diffusion Flames, Combust. Sci. Tech. Vol. 53 (1987), pp. 203-218.

[8] B.S. Haynes and H.Gg. Wagner: Soot Formation, Prog. Energy Combust. Sci. Vol. 7 (1981), pp. 229-273.

[9] I. Glassman: Soot Formation in Combustion Processes, Twenty-Second Symposium (International) on Combustion, The Combustion Institute, Pittsburgh, 1988, pp. 295-311.

[10] B. Rogg: On Numerical Analysis of Two-Dimensional, Axisymmetric, Laminar Jet Diffusion Flames, Mathematical Modeling in Combustion and Related Topics (C.-M. Brauner and C. Schmidt-Laine, eds.), Martinus Nijhoff Publishers, Amsterdam, 1988, pp. 551-560.

[11] M.D. Smooke, R.E. Mitchell and D.E. Keyes: Numerical Solution of Two-Dimensional Axisymmetric Laminar Diffusion Flames, Combust. Sci. Tech. Vol. 67 (1989), pp. 85-122.

[12] R.W. Bilger: Reaction Rates in Diffusion Flames, Combust. Flame Vol. 30 (1977), pp. 277-284.

[13] J.P. Gore and G.M. Faeth: Structure and Spectral Radiation Properties of Turbulent Ethylene/Air Diffusion Flames, Twenty-First Symposium (International) on Combustion, The Combustion Institute, Pittsburgh, 1986, pp. 1521-1531.

[14] J.P. Gore and G.M. Faeth: Structure and Radiation Properties of Luminous Turbulent Acetylene/Air Diffusion Flames, J. Heat Trans. Vol. 110(1988), pp. 173-181.

[15] Y.R. Sivathanu and G.M. Faeth: Generalized State Relationships for Scalar Properties in Nonpremixed Flames, Combust. Flame Vol. 82 (1990), pp. 211-230.

[16] K.P. Schug, Y. Manheimer-Timnat, P. Yaccarino, and I. Glassman: Sooting Behavior of Gaseous Hydrocarbon Diffusion Flames and the Influence of Additives, Combust. Sci. Tech. Vol. 22 (1980), pp. 235-250.

[17] Y.R. Sivathanu and G.M. Faeth: Soot Volume Fractions in the Overfire Region of Turbulent Diffusion Flames, Combust. Flame Vol. 81 (1990), pp. 133-149.

[18] W.L. Flower and C.T. Bowman: Soot Production in Axisymmetric Laminar Diffusion Flames at Pressures from One to Ten Atmospheres, Twenty-First Symposium (International) on Combustion, The Combustion Institute, Pittsburgh, 1986, pp. 1115-1124.

[19] S. Gordon and B.J. McBride, Computer Program for Calculation of Complex Chemical Equilibrium Composition, Rocket Performance, Incident and Reflected Shocks, and Chapman-Jouget Detonations, NASA SP-273, Washington, 1971.

[20] S.V. Patankar: Numerical Heat Transfer and Fluid Flow, McGraw-Hill, New York, 1980.

[21] D.B. Spalding: Combustion and Mass Transfer, Pergamon Press, New York, 1979, Chapt. 10.